Journal of Drug Delivery Science and Technology 121 (2026) 108354

Contents lists available at ScienceDirect

Journal of Drug Delivery Science and Technology

journal homepage: www.elsevier.com/locate/jddst

Nature-based nanostructured lipid carriers containing β-caryophyllene for skin cancer adjuvant therapy: Development and study of their bioactivities *in vitro*

Maria Eduarda Lima Dano [a], Hélen Cássia Rosseto [b], Maddalena Sguizzato [c], Francesca Ferrara [c], Rita Cortesi [c], Mariana Carla de Oliveira [a], Rodolfo Bento Balbinot [d], Celso Vataru Nakamura [d], Lidiane Vizioli de Castro-Hoshino [e], Mauro Luciano Baesso [e], Marcos Luciano Bruschi [a,*]

[a] *Laboratory of Research and Development of Drug Delivery Systems, Postgraduate Program in Pharmaceutical Sciences, Department of Pharmacy, State University of Maringa, Maringa, PR, Brazil*
[b] *College of Pharmaceutical Sciences, Food and Nutrition, Federal University of Mato Grosso do Sul, Campo Grande, MS, Brazil*
[c] *Department of Chemical, Pharmaceutical and Agricultural Sciences, University of Ferrara, Ferrara, Italy*
[d] *Technological Innovation Laboratory in the Pharmaceuticals and Cosmetics Development, State University of Maringa, Maringa, PR, Brazil*
[e] *Department of Physics, State University of Maringa, Maringa, Parana, Brazil*

ARTICLE INFO

Keywords:
Lipid systems
Topical drug delivery
Passion fruit oil
Soy lecithin
Permeation

ABSTRACT

Modern medicine has made significant progress by incorporating natural bioactive compounds, not only as active ingredients but also as functional excipients. This study aimed to develop naturally derived nanostructured lipid carriers (NLCs) containing β-caryophyllene as a therapeutic adjuvant for the treatment of skin cancer. To identify the optimal combination among passion fruit oil, beeswax, soy lecithin, and β-caryophyllene, a component screening was performed. The formulations' stability was monitored by particle size analysis and macroscopic evaluation over 30 days. Transmission electron microscopy of the optimized systems revealed the typical spherical morphology of NLCs. They exhibited drug entrapment efficiency higher than 92%. The lipid matrix, surrounded by the surfactant layer, effectively protected β-caryophyllene from volatilization. The release profile appeared to follow anomalous transport behavior. Photoacoustic spectroscopy indicated that β-caryophyllene could permeate into the dermis. Two selected systems (F3 and F21) enhanced the cytotoxic selectivity of β-caryophyllene against representative melanoma cells (B16-F10), with selectivity indices of 2.07 and 2.2, respectively. Overall, the developed systems demonstrated physicochemical and therapeutic characteristics that support their potential as adjuvants for the topical treatment of skin cancer. Future *in vivo* studies are warranted to confirm this potential.

1. Introduction

According to the World Health Organization (WHO), non-melanoma skin cancer (NMSC) is the fifth most prevalent form of cancer worldwide [1]. It typically affects cells in the basal layer (basal cell carcinoma) or the spinous layer (squamous cell carcinoma) [2]. However, skin cancer may also originate from melanocytes, giving rise to melanoma, which is considered the most aggressive form of the disease [3].

Chemotherapy remains one of the primary treatment options for both forms, as it can target tumor cells at various stages of the cell cycle and act on multiple sites simultaneously [4,5]. Nevertheless, the systemic action of chemotherapeutic agents is not limited to cancer cells; healthy cells are also affected, leading to adverse effects for the patient [6,7].

One strategy to minimize these side effects is to reduce the chemotherapy dose. However, when implemented in isolation, such dose reduction may compromise the treatment's effectiveness and overall cure rate [8–12]. Alternatively, combining chemotherapy with complementary compounds may allow for a reduction in the conventional drug dose, as these compounds can enhance the therapeutic effect

* Corresponding author.
E-mail address: mlbruschi@uem.br (M.L. Bruschi).

https://doi.org/10.1016/j.jddst.2026.108354
Received 7 October 2025; Received in revised form 30 March 2026; Accepted 19 April 2026
Available online 20 April 2026
1773-2247/© 2026 The Authors. Published by Elsevier B.V. This is an open access article under the CC BY license (http://creativecommons.org/licenses/by/4.0/).

without increasing adverse reactions.

In this context, terpenes are considered promising adjuvants for melanoma treatment, as several of them are capable of inducing apoptosis in cancer cells [13–15]. One such compound is β-caryophyllene (BCP) [16,17], a sesquiterpene found in copaiba, oregano, cinnamon, basil, and lavender [18]. In addition to its antitumor properties, BCP exhibits anti-inflammatory [19], antimicrobial [20], antioxidant, and analgesic [21] activities. Furthermore, Legault and Pichette (2010) demonstrated that BCP can promote the intracellular accumulation of the chemotherapeutic agent paclitaxel in colon cancer cells and enhance its activity in murine fibroblasts [22], highlighting its potential as a comprehensive and effective agent in skin cancer treatment.

However, due to its volatility and susceptibility to degradation by environmental factors such as light, hydrolysis, oxidation, and heat, administering BCP in its raw form is not suitable. Incorporating this nonpolar molecule into nanostructured lipid carriers (NLCs) through nanotechnology enables safer handling, enhanced stability, and improved bioavailability at the target site [23].

For topical application in skin cancer treatment, NLCs offer improved skin permeability due to their size and composition. Their affinity and structural similarity to the lipids of the stratum corneum suggest minimal skin irritation [7], while also facilitating lipid rearrangement. This promotes deeper penetration and increases the retention of active compounds within the skin layers [24–27]. Moreover, the biodegradable composition of NLCs and the absence of organic solvents in their preparation make these systems ecologically friendly [28].

In alignment with the United Nations Sustainable Development Goals (SDGs), which advocate for substantial waste reduction through prevention, minimization, recycling, and reuse [29], modern medicine has increasingly benefited from bioactive compounds derived from natural products. These compounds serve not only as active ingredients but also as excipients [30–32].

In this context, the use of natural raw materials contributes not only to the sustainability of the developed systems but also to their structural integrity and therapeutic potential.

Therefore, the present study aimed to develop NLCs composed exclusively of natural raw materials: natural wax, vegetable oil, soy lecithin, and BCP. This strategy employs renewable and biocompatible compounds to enable the topical application of BCP as an adjuvant for skin cancer treatment, enhancing its delivery to deeper skin layers and reducing its volatility, in accordance with the SDGs principles. The NLCs were also evaluated for *ex vivo* skin permeation and *in vitro* biological activities.

2. Materials and methods

2.1. Materials

Pluronic F68® (poloxamer 188) and β-caryophyllene (BCP; standard, purity ≥80%) were acquired from Sigma-Aldrich (Sao Paulo, SP, Brazil). Acetic acid was obtained from Synth (Diadema, SP, Brazil), and acetonitrile (HPLC grade) from *ACS Cientfica*. Beeswax was purchased from *All Chemistry do Brasil* (Sao Paulo, SP, Brazil), carnauba wax from *Comércio e Indústria Farmos* (Rio de Janeiro, RJ, Brazil), soy lecithin powder from *Dinâmica Contemporânea*, andiroba oil from *Mercado Ver-o-peso* (Belém, PA, Brazil), and copaiba oil-resin from *Copaíba da Amazônia*® (Guaruja, SP, Brazil). Passion fruit oil was extracted by cold pressing the fruit seeds by the company *Verde para sempre* (Salvaterra, PA, Brazil). Ultra-purified water was obtained in-house using a water purification system (Evoqua Water Technologies, Pittsburgh, PA, USA).

2.2. Preliminary compatibility studies

2.2.1. Lipid screening

Compatibility among the compounds plays a crucial role in the stability of the system. To assess the solubility between the solid lipids (beeswax or carnauba wax) and the liquid lipids (passion fruit oil, andiroba oil, or copaiba oil), a test was performed following the guidelines of the Brazilian Pharmacopoeia [33] and the described by Tamjidi et al. [34]. For this evaluation, 1 g of solid lipid was dispersed into 1 mL of liquid lipid in a beaker. The mixture was heated on a hot plate until the solid lipid was completely melted. After complete solidification at 25 °C, the sample was placed against a black background for visual inspection. Among the six combinations tested, the optimal formulation was selected for the subsequent "solubility of BCP in liquid lipid" test based on its solid and homogeneous appearance. The ideal combination should exhibit no phase separation or visible oil droplets [34].

2.2.2. Solubility of BCP in liquid lipid

Following the same procedures used for lipid screening, 1 g of the selected liquid lipid (passion fruit oil) was mixed with 1 mL of BCP. For comparison, 1 g of water, known to be practically insoluble with the bioactive compound, was also mixed with 1 mL of BCP. The resulting mixtures were visually examined for evidence of miscibility or phase separation.

2.3. Formulation pre-screening (lipid and surfactant combinations)

This step aimed at observing the effectiveness of a natural surfactant (soy lecithin) compared to a synthetic one (poloxamer 188) in stabilizing the NLCs system, as well as identifying the optimal solid-liquid lipid ratio (beeswax:passion fruit oil) based on the structural characteristics of formulations. The NLCs were prepared as described in Section 2.4.1. Formulations containing 4% (w/w) surfactant and 5% (w/w) total lipid, varying both the surfactant type (poloxamer 188 or soy lecithin) and the solid-liquid lipid ratios (6:4, 7:3, and 8:2). Although this preliminary screening did not yield formulations with ideal properties, it provided valuable insights into the surfactant capacity of soy lecithin and the influence of the solid-to-liquid lipid ratio. Based on the macroscopic analysis, these parameters were established for the development of the factorial design described below.

2.4. Design of Experiments (DoE) for optimizing the NLCs

Based on the previous findings, a 3^3-factorial design was developed to optimize surfactant concentration (X_1), total lipid content (X_2), and BCP content (X_3), according to Table 1.

2.4.1. Preparation of NLCs

The surfactant solution was first prepared by gradually dispersing lecithin or poloxamer 188 into purified water, under constant magnetic stirring. This solution was then heated to 70 °C, considering that the melting point of beeswax is from 63.5 to 64.5 °C [35,36]. Meanwhile, the beeswax and passion fruit oil were weighed and heated separately to the same temperature. Once both phases reached 70 °C, the lipid phase was added to the aqueous surfactant solution, forming a microemulsion. The mixture was homogenized using an Ultra-Turrax T10 basic (IKA, Staufen, Germany) at 15,000 rpm for 1 min, followed by sonication in a CPX-750 sonicator (Cole Parmer, Vernon Hills, IL, USA), for 5 min, at 20% amplitude and 20 kHz frequency. After preparation, the formulations were stored at room temperature to allow partial solidification and the formation of NLCs [37–39].

The macroscopic aspect of the systems was monitored for 30 days, and the systems were classified as (+++) very good, (++) good, (+) fair, (±) unsatisfactory or (−) poor. The system was considered very good (+++) when it was homogeneous and without agglomeration of particles; good (++) when there was very slight marking of adhered particles on the bottle wall; fair (+) when presented small agglomerates and a ring of particles adhered to the bottle wall; unsatisfactory (±) when it was not so homogeneous, with agglomerates of larger particles and the ring of particles; and poor (−) when there was an evident phase

Table 1
Factorial design (3^3) used for the NLCs design with different amounts of lipid, soy lecithin, and β-caryophyllene (BCP).

Independent variables	Levels		
	Low (−1)	Central (0)	High (+1)
X_1 = Lecithin content (%, w/w)	1.50	2.00	2.50
X_2 = Lipid content (%, w/w)	1.00	1.50	2.00
X_3 = BCP content (%, w/w)	0.50	0.75	1.00

Standard run (Formulations)	Content (%, w/w)		
	X_1	X_2	X_3
F1	1.50	1.00	0.50
F2	1.50	1.00	0.75
F3	1.50	1.00	1.00
F4	1.50	1.50	0.50
F5	1.50	1.50	0.75
F6	1.50	1.50	1.00
F7	1.50	2.00	0.50
F8	1.50	2.00	0.75
F9	1.50	2.00	1.00
F10	2.00	1.00	0.50
F11	2.00	1.00	0.75
F12	2.00	1.00	1.00
F13	2.00	1.50	0.50
F14	2.00	1.50	0.75
F15	2.00	1.50	1.00
F16	2.00	2.00	0.50
F17	2.00	2.00	0.75
F18	2.00	2.00	1.00
F19	2.50	1.00	0.50
F20	2.50	1.00	0.75
F21	2.50	1.00	1.00
F22	2.50	1.50	0.50
F23	2.50	1.50	0.75
F24	2.50	1.50	1.00
F25	2.50	2.00	0.50
F26	2.50	2.00	0.75
F27	2.50	2.00	1.00

separation.

2.4.2. Analysis of particle size and polydispersity index of NLCs

The samples were diluted 1:50 (v/v) in purified water, transferred to polystyrene cuvettes, and placed into the chamber of a Litesizer 500 instrument (Anton Paar GmbH, Graz, Austria). Using the dynamic light scattering (DLS) technique, a laser beam was directed to the nanoparticles at a 90° angle, allowing their size to be calculated based on the scattered light [40]. The Kalliope software (Anton Paar) converted these measurements into nanometers and determined the polydispersity index (PDI). Analyses were performed in triplicate at 25 °C after 1 day, 15 days, and 30 days of preparation.

2.5. Morphological analysis of NLCs by transmission electron microscopy (TEM)

The morphological evaluation of the three selected NLCs was performed to analyze their physical and structural characteristics using TEM technique. For sample preparation, a drop of each formulation was deposited onto a TEM grid coated with formvar film. After 1 min, the excess liquid was removed with filter paper, leaving a thin layer of the sample on the support substrate. A drop of 2% phosphotungstic acid was then applied for 1 min to stain the NLCs and enhance their surface contrast. The excess stain was removed, and the grids were examined using a TALOS L120C G2 Transmission Electron Microscope (Thermo Fisher Scientific, Eindhoven, Netherlands).

2.6. Analysis of BCP trapping efficiency

To determine the entrapment efficiency (EE%) of NLCs, 0.2 mL of each formulation was transferred to a 10 kDa filter (Fig. 1- Step 1). The filter was then placed into an Ultra 0.5 Amicon® microtube (Merck KGaA, Darmstadt, Germany) and centrifuged at 14,000×*g* for 20 min at 25 °C using a Z36 HK centrifuge (Wehingen, Germany) [41].

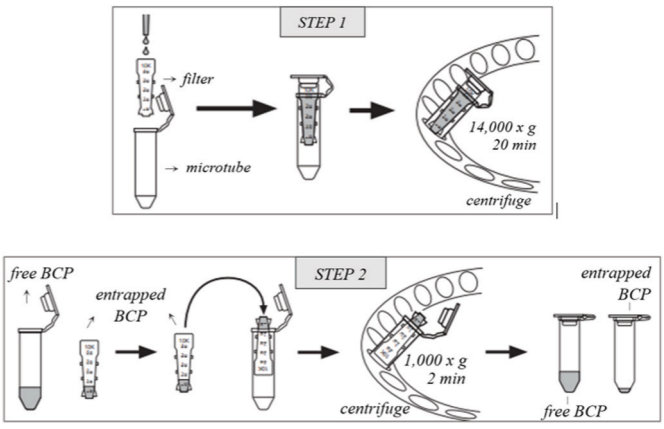


Fig. 1. Procedure for determining the entrapment efficiency (EE%) of NLCs containing BCP [41].

Afterward, the filter was inverted into another microtube, and centrifuged again, this time at 1000×*g* for 2 min at 25 °C (Fig. 1- Step 2) [41]. The aliquot collected at the end of Step 1 represents the amount of BCP that passed through the filter, corresponding to the free fraction not entrapped within the NLCs. This aliquot was then transferred to a 5 mL volumetric flask.

The fraction obtained in Step 2 corresponds to the material retained on the filter, consisting of the NLCs loaded with BCP. This fraction was transferred to a 25 mL volumetric flask, and the volume in both flasks was completed with acetonitrile. The samples were then filtered and quantified using high-performance liquid chromatography (HPLC), following the methodology described by Oliveira and collaborators [42,43]. A Prominence-i LC-2030C HPLC system (Shimadzu, Tokyo, Japan) equipped with a column oven (model FCV-14AH), automatic sample injector, and photodiode array detector was used. Analyses were performed at 22 °C with an injection volume of 20 µL, and detection was carried out at wavelength (λ) of 210 nm. A Supelcosil LC-18 (25 cm × 4.6 mm, 5 µm; Supelco, Saint Louis, MO, USA) coupled to a Gemini C18 guard column (4 × 3 mm; Phenomenex, Torrance, CA, USA) was employed. The mobile phase consisted of acetonitrile (Phase A) and ultrapure water containing 0.1% (v/v) acetic acid (Phase B), at a flow rate of 1.0 mL/min. The total run time was 25 min, using the following gradient elution (Phase A:Phase B, %) was: 60:40 (0-2 min); 65:35 (2-4 min); 70:30 (4-6 min); 75:25 (6-8 min); 80:20 (8-10 min); 100:0 (10-12 min); 70:30 (12-25 min). Chromatograms and analytical parameters were processed using LabSolutions version LC Solution Lite software (Shimadzu, Tokyo, Japan).

The BCP entrapment efficiency (EE%) was calculated according to Eq. (1) [44]:

$$EE\% = \frac{Total\ amount\ of\ BCP - Amount\ of\ free\ BCP}{Total\ amount\ of\ BCP}\ x\ 100 \quad (1)$$

where *EE%* is the entrapment efficiency.

2.7. In vitro analysis of BCP release profile from NLCs

The *invitro* release profile was evaluated using 12-well Corning® Transwell® plates equipped with 8-µm pore polyester membrane inserts (MilliporeSigma, Merck KGaA, Darmstadt, Germany) [45]. An amount of each formulation equivalent to 0.18 mg of BCP was calculated, weighed, and placed into the inserts: 18.4 mg for formulations F3 and F21, 24.4 mg for F11, and 0.18 mg for free BCP. The inserts were then carefully positioned in wells containing 0.6 mL of a water:ethanol

mixture (1:1, v/v), used as the dissolution medium. This medium was selected to ensure adequate drug solubility and maintain sink conditions throughout the experiment. The plates were incubated in an orbital shaker at 100 rpm and 34 °C for 8 h.

Samples of 0.2 mL were collected at predetermined intervals (after 30 min, 1 h, 2 h, 3 h, 4 h, 6 h, and 8 h), and the volume was immediately replaced with the dissolution medium. Each collected aliquot was transferred to a 1.0 mL volumetric flask, diluted with acetonitrile, filtered through a 0.45 μm PTFE membrane, and placed into vials for quantification. The released BCP was quantified by HPLC analysis as previously described. All experiments were performed in, at least, three replicate samples, and the results were expressed as both absolute and cumulative amounts of BCP released at each time point, considering the actual content of BCP in the formulations [46]. Furthermore, the release profiles were analyzed according to the Korsmeyer-Peppas mathematical model to investigate the release kinetics, as described by Eq. (2) [47,48]:

$$\frac{Mt}{M\infty} = k.t^n \quad (2)$$

where: $\frac{Mt}{M\infty}$ is the amount of drug released considering the time t; t is the release time; k is the kinetic constant of incorporation of structural and geometric characteristics of the release device; n is the exponent indicating the drug release mechanism.

The dissolution profile of free drug was also investigated for comparisons, in order to evaluate the effect of the carrier system on BCP release.

2.8. Ex vivo analysis of BCP permeation profile using photoacoustic spectroscopy

The skin permeation study was conducted using photoacoustic spectroscopy and ear skin obtained from recently slaughtered young albino pigs. Skin samples from the dorsal region of the ear were washed, the hair was removed, and the dermis and epidermis were dissected using a scalpel [49,50].

Photoacoustic spectroscopy was performed on the skin before and 30 min after the application of the formulations (F3, F11, and F21) or free BCP to the stratum corneum. The light source consisted of a xenon arc lamp (Oriel, model 68820) with a nominal power of 800 W, capable of reaching up to 1000 W. The emitted light was directed to a monochromator (Oriel, model 77250) equipped with 3.16 mm entrance and exit slits and a diffraction grating (Oriel, model 77296) for spectral acquisition in the UV-Vis range (220 to 450 nm). The light was modulated by a mechanical chopper (Stanford Research Systems, model SR 540) at a frequency of 13 Hz. Band-pass filters were used to eliminate higher-order diffractions. The modulated light beam was directed onto the sample, which was positioned inside the photoacoustic cell and sealed with a transparent quartz window (8 mm diameter and 2 mm thickness). The pressure variations generated by heating the sample upon absorption of the modulated light produced a photoacoustic signal, which was detected by a capacitive microphone (Brüel and Kjaer, model 2669). A lock-in amplifier (EG&G Instruments model 5110) was used to detect and amplify the corresponding signal [51]. The tissue thickness contributing to the photoacoustic signal was calculated based on the thermal diffusion length (μ_s), according to Eq. (3) [52].

$$\mu_s = (D/\mu f)^{1/2} \quad (3)$$

Where μ_s is the thermal diffusion length, D is the thermal diffusivity of the sample (4.1×10^{-4} cm^2/s), and μf is the light modulation frequency (13 Hz). Consequently, μ_s was 31 μm for the skin, ensuring that readings were taken close to the surface where the light was incident. The average sample thickness was consistently around 1080 μm.

2.9. In vitro cytotoxicity and antitumoral activity studies

The cytotoxicity of formulations was evaluated using representative healthy skin cells: murine fibroblasts L-929 (ATCC CCL-1) and monkey kidney epithelial cells *(Cercopithecus aethiops)* VERO (ATCC CCL-81). Murine melanoma B16-F10 cells (CRL-6475™) were used for the investigation of antitumor activity.

Cells were cultured in 200 mL tissue culture flasks. B16-F10 cells were maintained in Roswell Park Memorial Institute 1640 medium (RPMI, pH 7.6), while VERO and L-929 cells in Dulbecco's Modified Eagle Medium (DMEM, pH 7.2), supplemented with 1% penicillin and streptomycin. Both media were enriched with L-glutamine and 10% fetal bovine serum (FBS). The tests were conducted under sterile conditions in a laminar flow hood and repeated three times in different weeks for each cell line.

2.9.1. Cell counting and seeding

Culture flasks previously incubated with the cells and medium were used as the source for counting and seed the cells for the assay. After removing the medium, adherent cells were washed with phosphate-buffered saline (PBS) and detached using 3 mL of trypsin solution, with exposure times of 20 s for B16-F10 cells and 1 min for VERO and L-929 cells. The enzymatic solution was then discarded, and 6 mL of culture medium were added to neutralize the trypsin. From this volume, 5 mL were transferred to a Falcon tube for cell counting and subsequent seeding.

An aliquot of 100 μL from the Falcon tube was diluted in 900 μL of medium, and 10 μL of this suspension were loaded into a Neubauer chamber for cell counting using an optical light microscope. Cell density (cells/mL) was determined based on the average count of the four quadrants, multiplied by the dilution factor (10) and divided by the quadrant volume (10^{-4} mL). Based on this result, the suspension was adjusted with medium and 10% FBS to a final concentration of 2.5×10^5 cells/mL. Subsequently, 100 μL of the adjusted cell suspension were seeded into each well of 96-well plates and incubated for 24 h at 37 °C in an 5% CO_2 atmosphere.

2.9.2. Cells treatment with NLCs and free BCP

The medium was removed from the wells and the formulations (F3, F3B, F11, F11B, F21, F21B, and BCP) were diluted with RPMI or DMEM for the treatment.

Following serial dilution, concentrations corresponding to 200 μg/mL, 100 μg/mL, 50 μg/mL, 25 μg/mL, 12.5 μg/mL and 6.25 μg/mL of BCP were prepared. Then, 100 μL of each concentration was added to the respective wells, with two wells for each concentration of each cell. The remaining wells were filled only with medium, serving as a control. The plates were incubated for 24 h at 37 °C and 5% CO_2. The medium in the plates was then removed again and replaced by 50 μL of a 2 mg/mL MTT (3-(4,5-Dimethylthiazol-2-yl)-2,5-Diphenyltetrazolium Bromide) solution in PBS. The plates were incubated for 4 h, under the same conditions as before. The MTT solution was then removed and 150 μL of dimethyl sulfoxide was added to each well to dissolve the precipitated formazan crystals. The plates were homogenized and analyzed in a plate spectrophotometer (Power Wave XS-BioTek) at 570 nm at 25 °C [53]. The percentage of viable cells was calculated, and the CC_{50} values (cytotoxic concentration at 50%) were determined by nonlinear regression analysis. The results were expressed as the mean ± standard deviation of at least three independent experiments.

2.10. Statistical analysis

The effects of independent variables (the content of lecithin, lipid and BCP) on the physicochemical properties of formulations, statistical analyzes were performed using the Statistica 10.0 software (StatSoft Company, Tulsa, OK, USA). For this purpose, the Design of Experiments (DoE) approach was applied, with Analysis of Variance (ANOVA), using

Tukey's Honestly Significant Difference. Normality, homogeneity of variance, homoscedasticity, and independence were evaluated. A significance level of $p < 0.05$ was adopted [54].

3. Results and discussion

3.1. Preliminary compatibility tests

Incorporating oil into the solid lipid core of lipid nanoparticles provides several advantages, including enhanced entrapment efficiency of the active agent, increased loading capacity, improved system stability, and more controlled drug release from this phase [34]. To achieve these benefits, the lipids must be mutually miscible and compatible with the active ingredient.

3.1.1. Lipid screening

Lipids are the primary components influencing the entrapment and release of the active agent [55]. Incompatibility among them results in poor system structuring and, consequently, ineffective drug delivery.

Formulations containing carnauba wax exhibited evident phase separation, indicating its inability to form a stable and homogeneous system with andiroba, copaiba, and passion fruit oils. The hardness and high melting point of carnauba wax (approximately 86 °C) [56] likely contributed to the formation of a solid, rigid, and slightly flexible structure after solidification. This structure did not integrate well with the oils, leading to the development of a heterogeneous system.

In contrast, beeswax, which has a lower melting point (63.5-64.5 °C), produced a macroscopically homogeneous appearance when mixed with the oils. The hydrocarbons present in this wax make it more nonpolar and malleable, which may have led to better interaction and compatibility with the liquid lipids [35].

Formulations containing copaiba oil exhibited certain peculiarities. The center of the mixture showed a more intense coloration than the edges, indicating a non-uniform distribution of components. This heterogeneity may be attributed to the complexity of copaiba oil, an oil-resin that is exceptionally rich in sesquiterpenes and diterpenes, making it chemically more intricate than the other oils used [57]. The interaction between the terpenes in copaiba oil and the lipids in beeswax may not have been fully compatible, potentially explaining the concentration of certain components at the ends of the mixture.

Thus, the most compatible combinations were those pairing beeswax with andiroba or passion fruit oil, both of which demonstrated successful component integration. Passion fruit oil produced a more uniform and brighter mixture and was therefore selected as the liquid lipid for system development.

3.1.2. Solubility of BCP in liquid lipid

BCP, a bicyclic sesquiterpene, has a highly apolar structure, which suggests a natural affinity with oils due to hydrophobic interactions [18]. The results showed that BCP formed a homogeneous mixture at a 1:1 (w/v) ratio with passion fruit oil, indicating high solubility [33]. Passion fruit oil, rich in fatty acids such as linoleic and oleic acid, provides a compatible medium for the dissolution of hydrocarbons like BCP. As expected, the combination with water exhibited phase separation. Good compatibility between the lipid vehicle and the therapeutic molecule can potentially enhance the compound's bioavailability in topical formulations.

3.2. Formulation pre-screening (lipid and surfactant combinations)

To ensure the homogeneity and stability of a system composed of two immiscible phases, the addition of a surfactant is essential. In NLCs systems, the surfactant must effectively reduce the interfacial tension between the lipid phase (composed of surfactant concentration must be appropriate. When it is insufficient, the lipid phase may not disperse completely and separate from the solution. In contrast, an excessive amount of surfactant may pose toxicity risks. Typically, acceptable concentrations for these systems range from 0.5 to 5% (w/w) [28,58].

Accordingly, the systems were prepared and compared based on their macroscopic characteristics. Immediately after preparation, formulations containing P188 exhibited small solid structures dispersed on the surface (Fig. 2), whereas those prepared with soy lecithin presented a smooth and uniform appearance. The presence of these structures may indicate that the lipid concentration (5%, w/w) was too high, that the surfactant amount was insufficient, or that incompatibility existed between the surfactant and the lipids.

Considering that both soy lecithin and P188 were used at the same concentrations (3.0, 3.5, and 4.0%, w/w) and that the lipid content was fixed at 5% (w/w), soy lecithin demonstrated superior performance when combined with beeswax and passion fruit oil. It resulted in a homogeneous surface, without agglomerates, leading to its selection for the systems in this study. Consequently, the resulting formulations will have a 100% natural composition, as soy lecithin is derived from soybean seeds (*Glycine max*) [59].

After one week, both the P188 and soy lecithin formulations displayed clumps of lipid particles on the vial surface, indicating instability. Physicochemical instability in emulsions may manifest through gravitational separation (creaming or sedimentation), flocculation, coalescence, or Ostwald ripening. Although nanoemulsions generally resist gravitational separation and flocculation, they are particularly susceptible to coalescence and Ostwald ripening. Ostwald ripening occurs when smaller droplets dissolve and redeposit onto larger ones, causing their growth. In contrast, coalescence takes place when two or more droplets merge into a single larger droplet as their interfaces break down [60,61]. The particle agglomeration observed after one week may be attributed to inadequate stabilization of the lipids by the surfactant, possibly due to an insufficient surfactant concentration to stabilize the 5% (w/w) lipids. Since increasing the surfactant content would not be desirable from toxicity standpoint, the lipid was reduced in Section 2.4.

Furthermore, the formulations that exhibited fewer signs of coalescence were F5 and F8, both containing lecithin and featuring a solid-to-liquid lipid ratio of 7:3. This ratio was therefore selected, as a higher proportion of solid lipid contributed to a more stable and cohesive matrix.

3.3. Design of experiment (DoE) for optimizing the NLCs

3.3.1. Preparation of NLCs

The NLC systems were prepared both with and without BCP for evaluation of the impact of its incorporation. Immediately after preparation, all formulations appeared fluid, homogeneous, and white in color, with no visible signs of particle agglomeration or solid residue on the surface of the vial (Fig. 3).

Reducing the lipid content in the formulations, along with adjusting the lecithin concentration in the aqueous phase, contributed to the development of nanoparticles that remained more stable over time. The

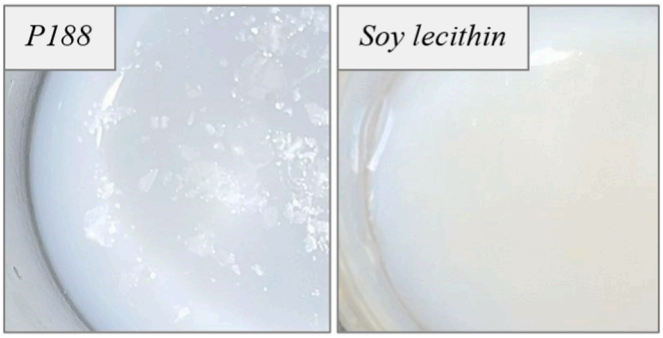


Fig. 2. Macroscopic characteristics of NLCs systems containing poloxamer 188 (P188) or soy lecithin.

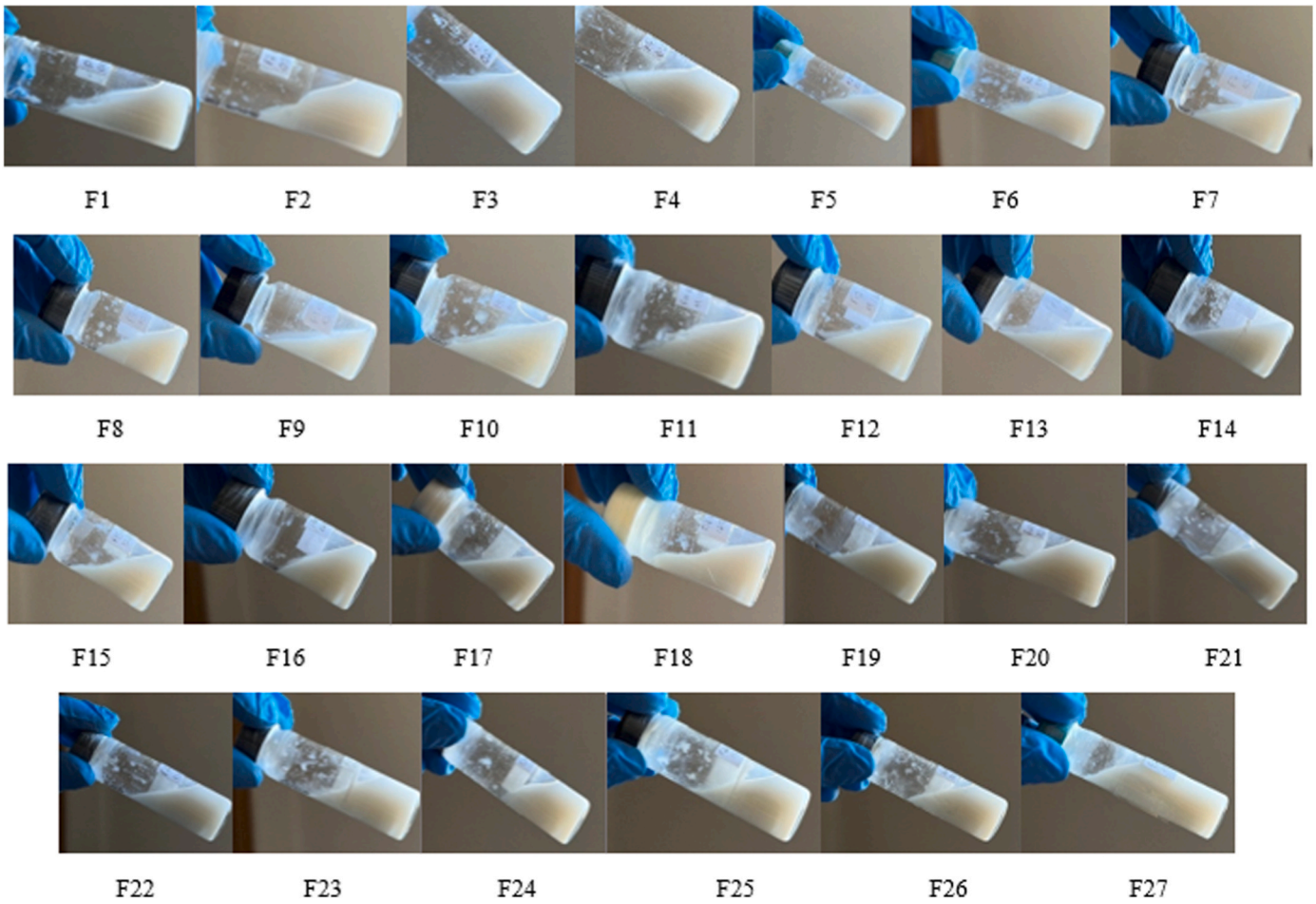


Fig. 3. Macroscopic characteristics of NLC systems prepared according to *DoE* and containing BCP (F1 to F27).

systems were monitored macroscopically for 30 days to evaluate the occurrence of coalescence or Ostwald ripening. A cross-evaluation scale

Table 2
Macroscopic analysis of formulations over 30 days, using cross signs (+) to describe the stability of the developed systems.

Formulation	1-day	7-days	15-days	30-days	Formulation	1-day	7-days	15-days	30-days
F1-F3B	++	++	++	+	F1	+++	+++	+++	++
					F2	+++	+++	+++	++
					F3	+++	+++	+++	+++
F4-F6B	++	++	+	±	F4	+	+	±	-
					F5	++	++	++	++
					F6	+	+	+	+
F7-F9B	++	++	+	+	F7	+++	+++	+++	++
					F8	++	+	+	+
					F9	+++	++	++	++
F10-F12B	++	++	++	+	F10	+++	+++	+++	++
					F11	+++	+++	+++	+++
					F12	+++	+++	+++	++
F13-F15B	+++	+++	+++	++	F13	+++	±	±	±
					F14	+++	-	-	-
					F15	+++	+++	+++	++
F16-F18B	++	+	±	-	F16	+++	+++	++	±
					F17	+++	+	+	±
					F18	+++	+++	++	++
F19-F21B	++	±	±	-	F19	+++	±	-	-
					F20	+++	+++	+++	±
					F21	+++	+++	+++	+++
F22-F24B	++	±	±	-	F22	++	-	-	-
					F23	++	-	-	-
					F24	+++	+++	+++	++
F25-F27B	±	±	±	±	F25	++	+	±	-
					F26	+++	+++	+++	±
					F27	++	++	+	+

(+++) Very good; (++) Good; (+) Fair; (±) Unsatisfactory; (−) Poor.

was employed for this analysis (Table 2).

Formulations F3, F11 and F21 remained stable even after 30 days of preparation and were therefore considered the most promising systems. The remaining formulations exhibited physical signs of instability, evidenced by particle agglomerations. Higher lipid concentrations were associated with an increased tendency for coalescence and lipid deposition on the inner walls of the tube. This behavior can be attributed to the greater likelihood of particle collisions as lipid content increases, promoting fusion and destabilization of the system.

Over the time, the tendency for particle agglomeration became more pronounced. The kinetic stability of the NLCs depends on the intermolecular interactions between lipids and the surfactant in the aqueous medium. However, these interactions may weaken over time, allowing the system's free energy to overcome the stabilizing forces, which can lead to droplet growth and loss of colloidal stability [60,61].

Formulations containing 1% (w/w) of lipids combined with 1.5; 2.0; or 2.5% (w/w) of soy lecithin and 0.75 or 1.0% (w/w) BCP were considered suitable for maintaining droplet dispersion and prevent coalescence. This combination likely promoted the formation of an effective interfacial barrier around the droplets, preventing coalescence and deposition.

The addition of BCP to the systems proved to be extremely advantageous, substantially improving the properties of the systems over time. After 30 days, none of the white formulations exhibited very good stability (+++). However, with the incorporation of BCP, even the formulations classified as poor (−), such as F19-F21B, showed significant improvement when 1% (w/w) of the molecule was added, with F21 achieving very good stability (+++) (F21). Moreover, as the amount of BCP in the formulation increased, the macroscopic characteristics improved, suggesting that this molecule enhanced the interaction between lecithin and solid lipids.

3.3.2. Particle size analysis and polydispersity index of NLCs

The particle size of the NLCs ranged from 172 nm to 298 nm, while the PDI varied from 0.16 to 0.31. The raw dependent variables are provided in the Supplementary Material (Tables S1 and S2). Statistical analysis revealed that the most influential factor affecting the properties evaluated was the BCP concentration ($p < 0.05$). As the amount of BCP increased, both particle size and PDI decreased (Fig. 4). Because the PDI reflects the number of particle size populations within a sample, a lower PDI indicates a more homogeneous system [40]. This, in turn, enhances the reliability of the administered drug dose and ensures more consistent system performance.

Time did not exert a statistically significant influence on most systems ($p > 0.05$) (Fig. 5).

Over the 30-day evaluation period, the formulations that exhibited the greatest changes in average particle size were F14 and F22, which increased by approximately 20 nm and 30 nm, respectively, after 15 days. However, by the end of 30-day period, the particle size nearly returned to the initial values. A similar pattern was reported by Asadinezhad and collaborators, who observed a substantial increase in droplet size (around 50 nm) during the first 15 days of storage, followed by a reduction and stabilization by day 35. This behavior may be related to the high energy involved in NLCs preparation [60,62,63]. After 1 min of shear using an ultra-turrax at 15,000 rpm and 5 min of sonication at 20 kHz, the particles are initially mobile and unstable, requiring time to reach kinetic equilibrium. Thus, it was consistent that the dispersed particles in the developed NLCs exhibited slight size variations during the first few days before stabilizing.

Thus, the results obtained in this analysis not only confirmed the influence of BCP in reducing particle size and improving size homogeneity but also demonstrated that, despite minor early variations, the developed systems remained stable throughout the 30-day evaluation period.

3.4. Morphological analysis of NLCs by TEM

TEM analysis revealed the typical spherical morphology of NLCs [64], whether loaded with BCP or not (Fig. 6).

The particle sizes observed in the TEM images were consistent with the values obtained from the DLS analysis, which ranged from 150 to 300 nm. Some structures appeared smaller, while others were larger sizes, supporting the PDI values reported (0.16-0.31).

The difference in density within the NLCs may be related to the semicrystalline matrix formed by the lipid organization in the system. The interaction among beeswax, passion fruit oil, and BCP resulted in partial crystallization, promoting the formation of unstructured layers [44]. The well-defined contour surrounding the particles can be attributed to the lecithin coating, which stabilizes the interface between aqueous and lipid structures. Additionally, the irregular white areas observed near the particles are likely residues of the surfactant. When the systems are diluted with water at a 1:1 ratio, the white “cloud” tends to disappear (Fig. 7).

3.5. Analysis of the entrapment efficiency (EE%)

Determining the EE% of a system is essential for evaluating its quality and effectiveness in drug delivery. This parameter is directly influenced by the solubility of BCP in the lipid matrix and the ratio between lipids and surfactants. Moreover, EE% serves as an indicator of the efficiency of the preparation method, revealing whether any leakage, or in this case volatilization of the drug has occurred. The results revealed EE% values higher than 92%, indicating that the NLCs were highly effective in entrapping the BCP. It can also be observed that as the amount of lecithin increased (from F3 to F21), the EE% tended to rise (Table 3).

The only difference between F3 and F21 systems is the amount of lecithin (1.5% for F3 and 2.5% for F21), which is higher in F21. This

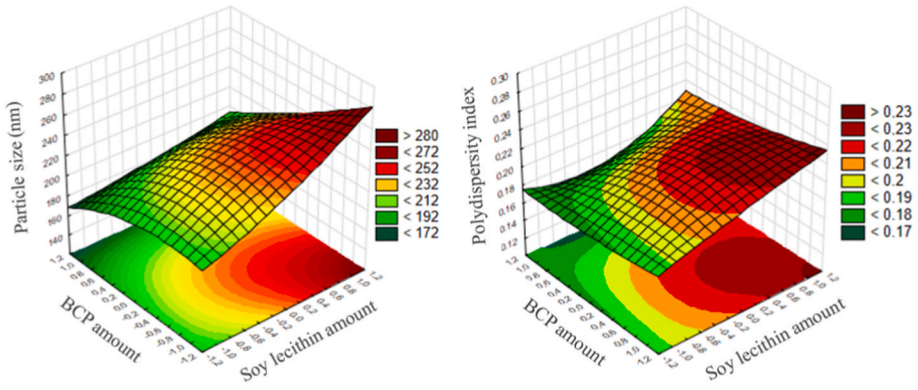


Fig. 4. Response surface plots of particle size and polydispersity index (PDI) of NLCs as a function of β-caryophyllene (BCP) and soy lecithin amount.

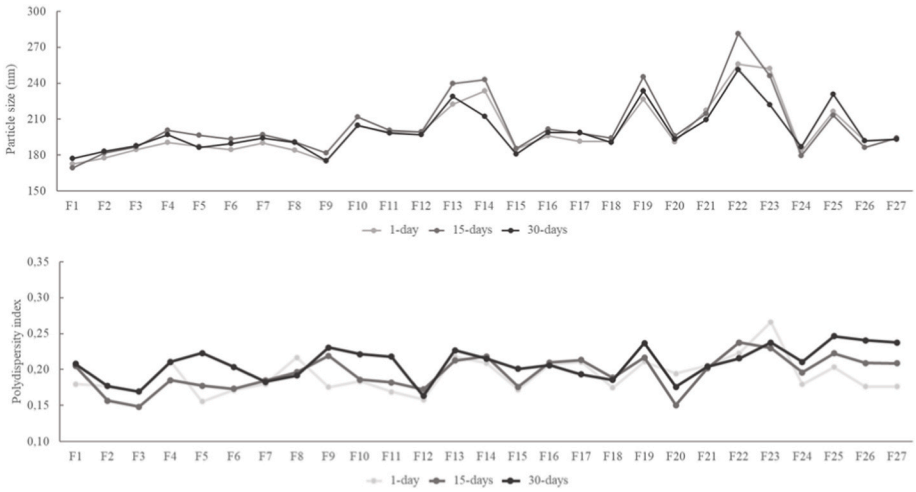


Fig. 5. Particle size and polydispersity index of NLC systems as a function of time for formulations F1-F27 prepared according to the *DoE*.

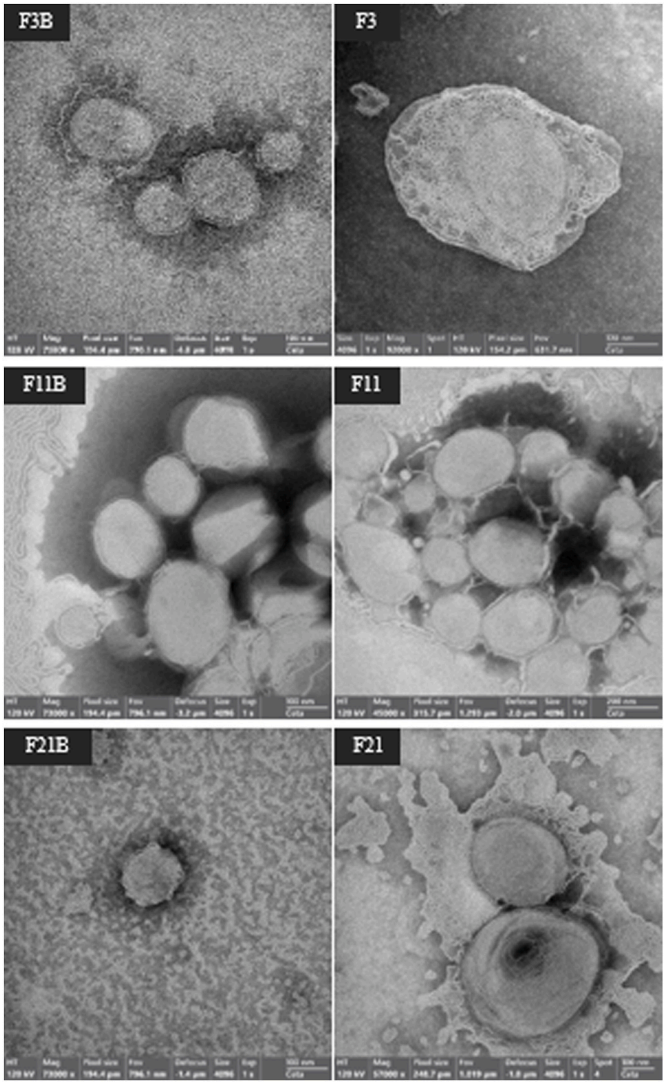


Fig. 6. Images obtained by transmission electron microscopy (TEM) of selected NLCs, with (F3, F11, and F21) and in the absence (F3B, F11B, and F21B) of BCP.

higher proportion of surfactant relative to the drug resulted in a 12% increase in EE%, reinforcing the essential role of lecithin in stabilizing

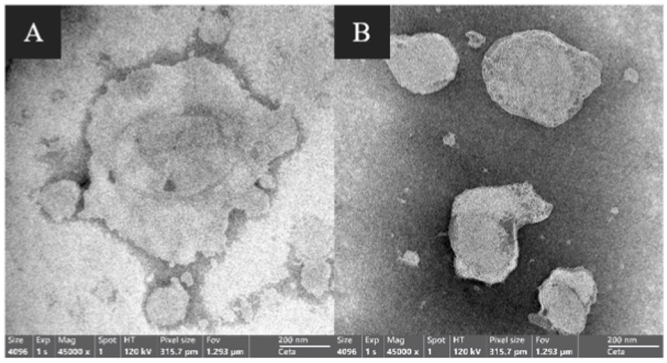


Fig. 7. Images obtained by transmission electron microscopy (TEM) of formulation F3 in its original concentration (A) and diluted in purified water (B).

Table 3
Entrapment efficiency (EE%) of NLCs containing BCP.

Formulation	EE (%, m/m)
F3	92.38 ± 2.03
F11	98.04 ± 1.74
F21	104.34 ± 0.72

the protective layer of the NLCs. This layer prevents the loss. Furthermore, higher lecithin concentrations increase the viscosity of the external phase and consequently reduce drug diffusion out of the matrix.

Thus, the EE of the developed systems reflects the success of the preparation method and enhances the therapeutic performance, as most of the drug remains available for controlled release.

3.6. *In vitro analysis of BCP release profile from NLCs*

To assess the impact of the lipid matrix on BCP release, the analysis compared free BCP with its nanostructured formulations. Free BCP showed a cumulative release of 39% over 8 h, whereas the NLCs released between 60% and 70% during the same period (Fig. 8).

These findings suggest that free BCP may have undergone rapid volatilization, even before crossing the release membrane. In contrast, the lipid systems appeared to protect the active compound, promoting a more efficient release profile. As a result, after 3 h, the NLCs released nearly twice as much BCP as the free molecule.

An increase in lecithin concentration (from F3 to F21) favored a

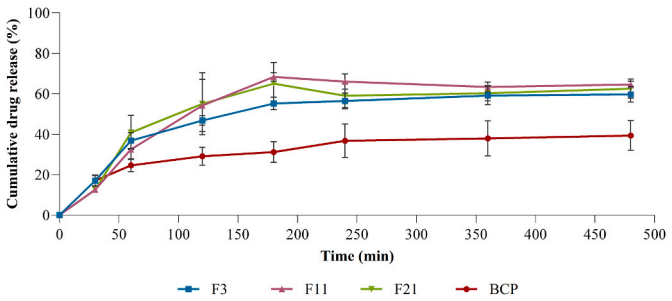


Fig. 8. Cumulative release profile of BCP: free and form the NLC systems F3, F11 and F21.

higher cumulative release over time, suggesting that lecithin not only can stabilize the interface but also contributes to prolong the drug release. According to the findings of Rosli and collaborators, the lipid formulations exhibit a rapid initial release of nearly 50% of the drug within the first 2 h, followed by a plateau, indicating a sustained or prolonged release profile. This release behavior may be attributed to the presence of a semicrystalline lipid matrix, which traps the drug and modulates its diffusion [65,66].

The Korsmeyer-Peppas kinetic model describes the release of bioactive molecules from matrix systems, which may occur through matrix erosion, dissolution, chain relaxation, or diffusion [48]. The release exponent (n) calculated by this mode indicates the predominant drug-release mechanism. For spherical geometries, such as nanoparticles, n values below than 0.43 indicate Fickian diffusion; values between 0.43 and 0.85 correspond to anomalous transport; and values above 0.85 represent Case II transport [67]. In this study, the free BCP molecule exhibited a diffusion exponent of $n = 0.29$ (Table 4), indicating a Fickian diffusion mechanism governed solely by the concentration gradient, in accordance with Fick's First Law [68].

The BCP release from formulation F3 ($n = 0.56$) was driven by anomalous transport, which involves both drug diffusion and chain relaxation. Formulations F11 and F21 exhibited n values close to one, demonstrated that chain relaxation predominates. It occurs as the lipid matrix swells, creating microcavities that allow the medium to diffuse into the matrix and facilitate the drug expulsion. As a result, a transition from a semi-rigid state to a more flexible one is observed [69].

The k values indicate the drug release rate, which is directly proportional to the speed of release during the first 60% of the process [48,68]. Free BCP showed the fastest release, since, as it is not trapped, its release occurs only through diffusion without needing to overcome the physical barriers of a matrix. In contrast, in nanostructured systems, the drug requires additional mechanisms to detach from the lipid matrix. It depends on the process of permeant diffusion and swelling.

For the medium to interact with the matrix and induce swelling, it must penetrate the lecithin layer around the particles. As the amount of lecithin increases, as observed in F11 and F21, the particle size also increases, suggesting reinforcement of this stabilizing layer. Consequently, the medium must cross thicker barrier to reach the matrix, resulting in a slower release rate compared with systems containing less (F3) or none at all (free BCP).

Thus, it was possible to establish a correlation between the lecithin concentration, the kinetic constant (k), and the release mechanism (n). In formulations with lower lecithin content, including the free BCP, the release was faster and primarily governed by diffusion. In contrast, as the lecithin concentration increased, the release rate decreased and became progressively controlled by matrix swelling.

Overall, these findings indicate that the lipid matrix not only protects BCP from volatilization but also modulates its release kinetics, enabling a sustained and controlled profile that enhances drug delivery at the site of action.

Table 4
Release kinetic parameters calculated by the Korsmeyer-Peppas mathematical model.
Release kinetic parameters for the BCP from NLC systems (F3, F11 and F21) and free BCP.

Formulation	Release kinetic parameters		
	n	k (min^{-1})	R^2
Free BCP	0.2923 ± 0.0672	7.0313 ± 2.1095	0.9746 ± 0.0115
F3	0.5601 ± 0.0730	3.1174 ± 1.0864	0.9553 ± 0.0258
F11	1.0202 ± 0.1740	0.4816 ± 0.2644	0.8935 ± 0.0712
F21	1.0331 ± 0.2094	0.5144 ± 0.2823	0.8935 ± 0.0054

3.7. *Ex vivo analysis of BCP permeation profile using photoacoustic spectroscopy*

Photoacoustic spectroscopy confirmed the presence of BCP in both the epidermis and dermis of skin samples. In the recorded spectra, absorption was observed in the 220–400 nm range for both the free BCP molecule and its NLC formulations. Based on the absorption intensity in the epidermis, the region where the formulation was applied, it was evident that the formulations containing higher concentrations of BCP (F3 and F21) exhibited stronger absorption than formulation F11, which contained a lower amount of the active compound (Fig. 9).

In the dermis, although there were no significant differences were observed among the formulations ($p > 0.05$), the largest absorption area corresponded to F3 (Fig. 9). This formulation exhibited smaller particle

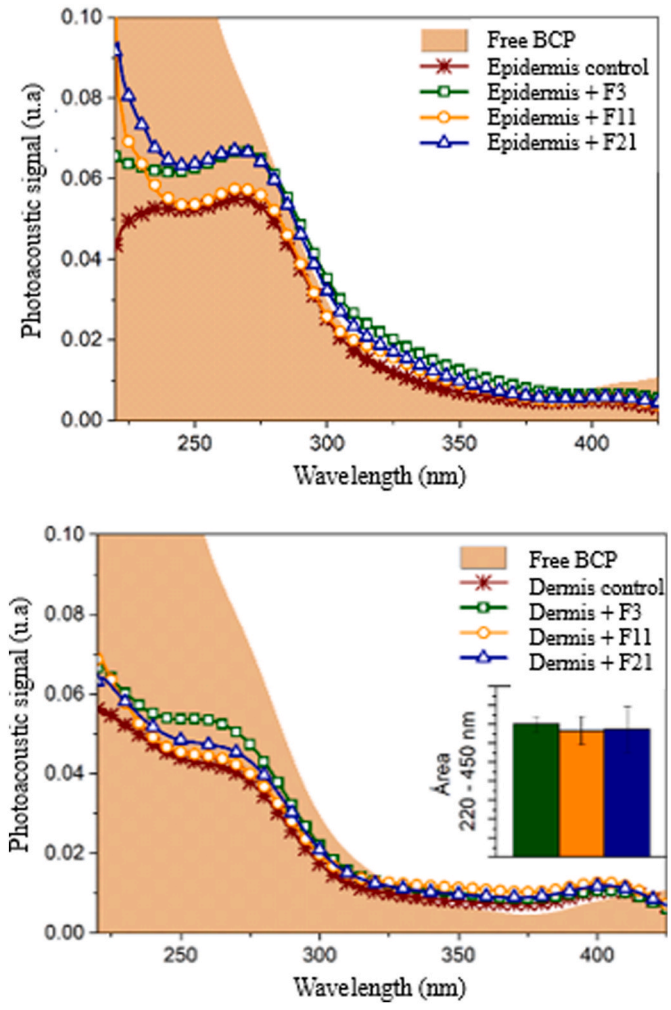


Fig. 9. Optical absorption spectra of the control epidermis, dermis, and 30 min after application of the formulations.

size compared with the others, suggesting that the nanometric dimensions favored permeation into deeper layers. The NLC systems, composed of lipids biocompatible with those of the skin, likely promoted lipid rearrangement upon contact with the lipophilic matrix of the stratum corneum, thereby facilitating drug permeation into the underlying layers [24–27]. Overall, the results indicate that the developed formulations were capable of delivering the BCP to both the epidermis and the dermis.

3.8. *In vitro cytotoxicity and antitumoral activity studies*

To be well accepted, a pharmaceutical system must be safe, effective, and of high quality. In this context, it is essential that the developed NLCs exhibit selectivity, that is, they should be toxic to skin cancer cells while remaining safe for healthy cells. To evaluate these aspects, assays were performed using cell lines representative of healthy skin (L-929 and VERO) and melanoma tumor cells (B16-F10).

The results for L-929 cells showed that the blank formulations maintained cell viability above 70% at all tested concentrations, demonstrating the low toxicity of the excipients used (Fig. 10). The free BCP molecule exhibited cytotoxicity only at 100 and 200 μg/mL. For the BCP-loaded formulations, the maximum safe dose was identified at 25 μg/mL, with a significant reduction in cell viability at higher concentrations. This behavior may be related to the characteristics of the nanostructured systems, which can enhance the apparent toxicity of BCP due to the lipid composition and the increased ability of nanoparticles to cross biological barriers, such as the cell membrane. Future studies are needed to confirm this hypothesis.

A similar pattern was observed in VERO cells: the blank formulations were deemed safe, the free BCP molecule remained non-toxic up to 100 μg/mL, formulation F3 was safe up to 25 μg/mL, and formulations F11 and F21 were safe only up to 12.5 μg/mL (Fig. 11).

Considering the two healthy cell lines analyzed, it can be inferred that the doses required to maintain at least 70% cell viability were 25 μg/mL for formulation F3 and 12.5 μg/mL for formulations F11 and F21. However, for the treatment of skin cancer, these doses must also be sufficiently cytotoxic to ensure the elimination of melanoma cells.

In this context, the F11 formulation did not produce satisfactory results. Although the 12.5 μg/mL concentration preserved cell viability above 70% in healthy cells, it also maintained similar viability levels in B16-F10 melanoma cells (Fig. 12). This formulation contains a lower amount of BCP (0.75%, w/w) and a relatively higher proportion of lecithin (2.0%, w/w). In contrast, formulations F3 and F21 showed reduced viability in tumor cells at concentrations considered safe for healthy cells, indicating greater selectivity [70].

Formulations without BCP were also non-toxic to B16-F10 cells, confirming that the antitumor activity of the formulations is related to BCP and not to the other components of the system. However, the BCP-free molecule did not show significant toxicity to melanoma cells, except at concentrations where it was also toxic to healthy cells. Thus, NLCs likely acted as promoters of BCP permeation across cell membranes, facilitating its entry into tumor cells and inducing cell death.

Lipid nanoparticles developed by Kelidari and collaborators exhibited similar behavior, as they significantly increased the efficacy of the drug used. These systems containing *Mentha longifolia* and *Mentha pulegium* essential oils were compared with the oils in their raw form regarding their cytotoxic activity in tumor cell lines (melanoma A-375, breast cancer MDA-MB-468, and MCF-7). The pure essential oil presented limited efficacy, and even at the highest concentration tested (1200 μg/mL), cell viability was greater than 55%, revealing insufficient activity to significantly inhibit the growth of the tumor cells tested. In contrast, the solid lipid nanoparticles containing the oils could reduce the cell viability to approximately 10%, even using a concentration reduced by half (600 μg/mL), suggesting that there was an increase in efficacy, due to the better cellular penetration of the oil provided by the lipid systems [71].

For each cell type tested, the concentration required to reduce cell viability by 50% (CC_{50}) was determined, along with the selectivity index (SI) comparing healthy and tumor cells (Table 5). A high CC_{50} value indicates low cytotoxicity, meaning that higher concentrations of the compound are necessary to reduce cell viability by 50%. This behavior was observed for both the blank formulations and the free BCP molecule, which also showed SI values close to 1.

The SI, calculated as the ratio between the CC_{50} of healthy cells (VERO and L-929) and the CC_{50} of tumor cells (B16-F10), reflects the ability of the system or molecule to act selectively on tumor cells. Values lower than 1 indicate that the compound is more toxic to healthy cells than to tumor cells. Values close to 1 suggest low selectivity, as observed for the BCP free molecule and formulation F11. Both undesirable outcomes. In contrast, higher SI values are preferred, as they indicate greater efficiency against tumor cells and reduced toxicity toward healthy cells.

Although formulations F3 and F21 did not exhibit exceptionally high SI values, the indices calculated between CC_{50} L-929 and CC_{50} B16-F10

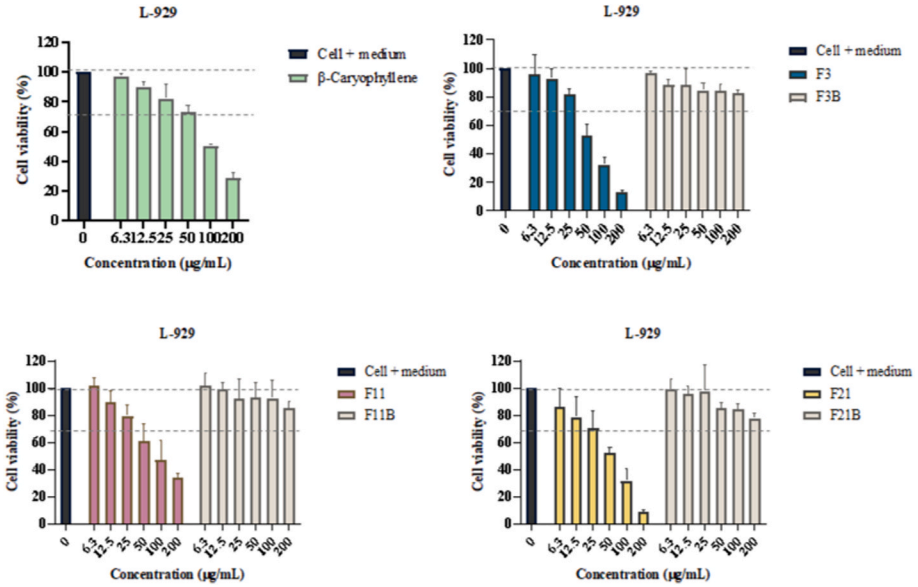


Fig. 10. Cell viability against L-929 cells provided by NLC systems F3, F11 and F21, their respective blanks and free β-caryophyllene (BCP), after 24 h of incubation.

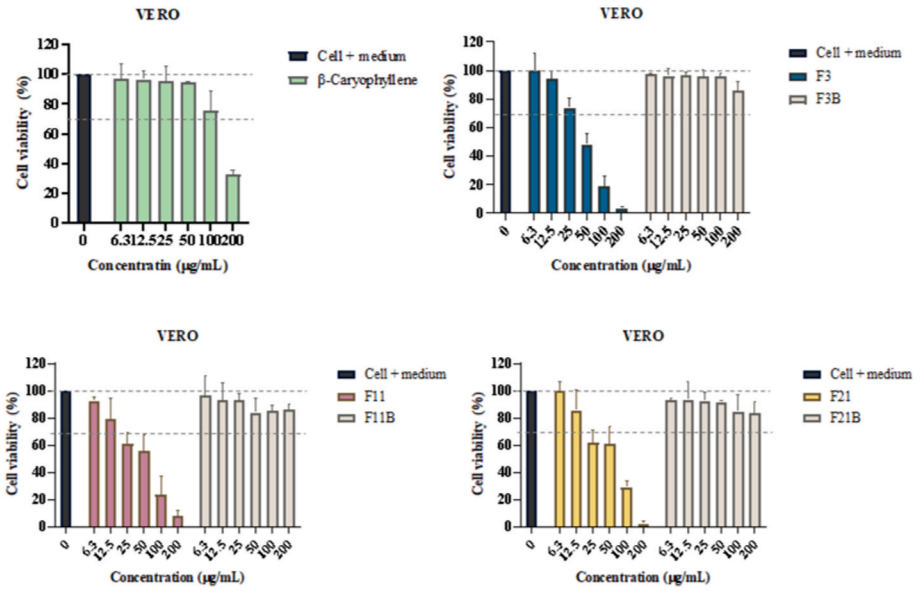


Fig. 11. Analysis of viability of VERO cells provided by NLC systems F3, F11 and F21, their respective blanks and free β-caryophyllene (BCP), after 24 h of incubation.

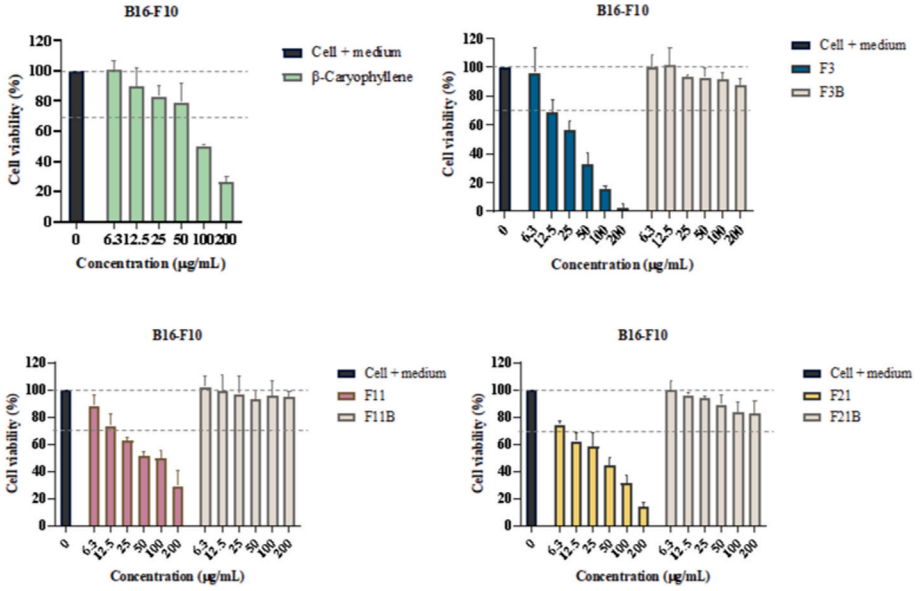


Fig. 12. Cell viability against B16-F10 cells provided by systems F3, F11 and F21, their respective blanks and free β-caryophyllene (BCP), after 24 h of incubation.

Table 5
Evaluation of the cytotoxic activity of lipid formulations containing β-caryophyllene (BCP).

Formulation	B16-F10	VERO		L-929	
	CC_{50} ± DP (µg/mL)	CC_{50} ± DP (µg/mL)	SI	CC_{50} ± DP (µg/mL)	SI
F3	30.19 ± 2.78	54.31 ± 3.27	1.8	62.55 ± 6.87	2.07
F3B	>200	>200	ND	>200	ND
F21	31.95 ± 2.64	59.81 ± 3.31	1.87	70.28 ± 5.49	2.2
F21B	>200	>200	ND	>200	ND
F11	55.84 ± 5.24	62.70 ± 8.72	1.12	73.44 ± 3.78	1.32
F11B	>200	>200	ND	>200	ND
BCP	102.47 ± 2.63	169.32 ± 17.68	1.65	114.71 ± 5.34	1.12

*CC_{50} = cytotoxic concentration for 50% of cells. SD = standard deviation. SI = selectivity index (CC_{50} VERO or L-929/CC_{50} B16-F10). ND = not determined.

were greater than 2. These values are nearly twice those observed for free BCP (IS = 1.12), demonstrating that the formulations enhanced the selective cytotoxicity of BCP.

Overall, these results indicate that the developed systems are promising candidates for the topical administration of BCP as a therapeutic adjuvant in skin cancer. To further improve selectivity, future

studies may explore the incorporation of additional compounds with complementary therapeutic potential.

4. Conclusion

The NLCs proved to be promising systems for the adjuvant topical treatment of skin cancer. Composed exclusively of natural raw materials, they exhibit ideal physicochemical characteristics, including appropriate particle size, low polydispersity index, and stability over 30 days, along with a controlled release profile and high encapsulation efficiency of BCP. In addition, the systems protected BCP from volatilization, enabled its permeation into the dermis, and enhanced drug's selectivity toward tumor cells. Thus, systems F3 and F21 were selected and identified as natural, safe, and effective candidates for adjuvant skin cancer therapy. Nevertheless, further *in vitro* and *in vivo* biological studies are required to validate their clinical applicability.

CRediT authorship contribution statement

Maria Eduarda Lima Dano: Conceptualization, Formal analysis, Investigation, Methodology, Writing – original draft. **Hélen Cássia Rosseto:** Investigation, Methodology. **Maddalena Sguizzato:** Investigation, Methodology. **Francesca Ferrara:** Investigation, Methodology. **Rita Cortesi:** Conceptualization, Methodology, Resources, Supervision. **Mariana Carla de Oliveira:** Formal analysis, Investigation, Methodology. **Rodolfo Bento Balbinot:** Formal analysis, Investigation, Methodology. **Celso Vataru Nakamura:** Conceptualization, Methodology, Resources. **Lidiane Vizioli de Castro-Hoshino:** Formal analysis, Investigation, Methodology. **Mauro Luciano Baesso:** Conceptualization, Methodology. **Marcos Luciano Bruschi:** Conceptualization, Funding acquisition, Methodology, Project administration, Resources, Supervision, Writing – review & editing.

Declaration of competing interest

The authors declare the following financial interests/personal relationships which may be considered as potential competing interests: Declarations of interest: none.

Acknowledgements

The authors are thankful to CAPES (*Coordenação de Aperfeiçoamento de Pessoal de Nível Superior*/Coordination for the Improvement of Higher Education of Brazil; Finance code 001). CNPq (*Conselho Nacional de Desenvolvimento Científico e Tecnológico*/National Counsel of Technological and Scientific Development of Brazil; Processes n°. 307695/2020-4 and 404163/2021-1) and FINEP (*Financiadora de Estudos e Projetos*/Financier of Studies and Projects of Brazil).

Appendix A. Supplementary data

Supplementary data to this article can be found online at https://doi.org/10.1016/j.jddst.2026.108354.

Data availability

Data will be made available on request.

References

[1] Instituto Nacional de Câncer, Estimativa 2023 : Incidência de Câncer no Brasil, 2022, p. 160.
[2] C.M. Treu, J.P. Almeida, O. Lupi, Câncer de pele: Manual teórico-prático, 1ed ed., Manole, Barueri, SP, 2021.
[3] L. Zeng, B.H.J. Gowda, M.G. Ahmed, M.A.S. Abourehab, Z.S. Chen, C. Zhang, J. Li, P. Kesharwani, Advancements in nanoparticle-based treatment approaches for skin cancer therapy, Mol. Cancer 22 (2023) 1–50, https://doi.org/10.1186/s12943-022-01708-4.
[4] M. Chaurasiya, G. Kumar, S. Paul, S.S. Verma, R.K. Rawal, Natural product-loaded lipid-based nanocarriers for skin cancer treatment: an overview, Life Sci. 357 (2024) 123043, https://doi.org/10.1016/j.lfs.2024.123043.
[5] R. Mouawad, M. Sebert, J. Michels, J. Bloch, J.-P. Spano, D. Khayat, Treatment for metastatic malignant melanoma: old drugs and new strategies, Crit. Rev. Oncol. Hematol. 74 (2010) 27–39, https://doi.org/10.1016/j.critrevonc.2009.08.005.
[6] S. Curran, M.M. Vantangoli, K. Boekelheide, J.R. Morgan, Architecture of chimeric spheroids controls drug transport, Cancer Microenviron. 8 (2015) 101–109, https://doi.org/10.1007/s12307-015-0171-0.
[7] H. Kaur, P. Kesharwani, Advanced nanomedicine approaches applied for treatment of skin carcinoma, J. Contr. Release 337 (2021) 589–611, https://doi.org/10.1016/j.jconrel.2021.08.003.
[8] G. Bonadonna, P. Valagussa, A. Moliterni, M. Zambetti, C. Brambilla, Adjuvant cyclophosphamide, methotrexate, and fluorouracil in node-positive breast cancer — the results of 20 years of Follow-up, N. Engl. J. Med. 332 (1995) 901–906, https://doi.org/10.1056/NEJM199504063321401.
[9] G. Bonadonna, P. Valagussa, Dose-response effect of adjuvant chemotherapy in breast cancer, N. Engl. J. Med. 304 (1981) 10–15, https://doi.org/10.1056/NEJM198101013040103.
[10] S.-H. Kuo, H.-C. Lien, S.-L. You, Y.-S. Lu, C.-H. Lin, T.-Z. Chen, C.-S. Huang, Dose variation and regimen modification of adjuvant chemotherapy in daily practice affect survival of stage I-II and operable stage III Taiwanese breast cancer patients, Breast 17 (2008) 646–653, https://doi.org/10.1016/j.breast.2008.05.006.
[11] A. Pearce, M. Haas, R. Viney, S.-A. Pearson, P. Haywood, C. Brown, R. Ward, Incidence and severity of self-reported chemotherapy side effects in routine care: a prospective cohort study, PLoS One 12 (2017) e0184360, https://doi.org/10.1371/journal.pone.0184360.
[12] W.C. Wood, D.R. Budman, A.H. Korzun, M.R. Cooper, J. Younger, R.D. Hart, A. Moore, J.A. Ellerton, L. Norton, C.R. Ferree, A.C. Ballow, E. Frei, I.C. Henderson, Dose and dose intensity of adjuvant chemotherapy for stage II, node-positive breast carcinoma, N. Engl. J. Med. 330 (1994) 1253–1259, https://doi.org/10.1056/NEJM199405053301801.
[13] P. Wróblewska-Łuczka, J. Cabaj, J. Bargieł, J.J. Łuszczki, Anticancer effect of terpenes: focus on malignant melanoma, Pharmacol. Rep. 75 (2023) 1115–1125, https://doi.org/10.1007/s43440-023-00512-1.
[14] S.H. Sharma, S. Thulasingam, S. Nagarajan, Terpenoids as anti-colon cancer agents – a comprehensive review on its mechanistic perspectives, Eur. J. Pharmacol. 795 (2017) 169–178, https://doi.org/10.1016/j.ejphar.2016.12.008.
[15] A. Modzelewska, S. Sur, S. Kumar, S. Khan, Sesquiterpenes: natural products that decrease cancer growth, Curr. Med. Chem. Agents. 5 (2005) 477–499, https://doi.org/10.2174/1568011054866973.
[16] L. Langhasova, V. Hanusova, J. Rezek, B. Stohanslova, M. Ambroz, V. Kralova, T. Vanek, J.D. Lou, Z.L. Yun, J. Yang, L. Skalova, Essential oil from Myrica rubra leaves inhibits cancer cell proliferation and induces apoptosis in several human intestinal lines, Ind. Crops Prod. 59 (2014) 20–26, https://doi.org/10.1016/j.indcrop.2014.04.018.
[17] A. Carracedo, M. Gironella, M. Lorente, S. Garcia, M. Guzmán, G. Velasco, J. L. Iovanna, Cannabinoids induce apoptosis of pancreatic tumor cells via endoplasmic reticulum stress–related genes, Cancer Res. 66 (2006) 6748–6755, https://doi.org/10.1158/0008-5472.CAN-06-0169.
[18] K. Fidyt, A. Fiedorowicz, L. Strządała, A. Szumny, B-Caryophyllene and B-Caryophyllene oxide—natural compounds of anticancer and analgesic properties, Cancer Med. 5 (2016) 3007–3017, https://doi.org/10.1002/cam4.816.
[19] R. Medeiros, G.F. Passos, C.E. Vitor, J. Koepp, T.L. Mazzuco, L.F. Pianowski, M. M. Campos, J.B. Calixto, Effect of two active compounds obtained from the essential oil of Cordia verbenacea on the acute inflammatory responses elicited by LPS in the rat paw, Br. J. Pharmacol. 151 (2007) 618–627, https://doi.org/10.1038/sj.bjp.0707270.
[20] B. Sabulal, M. Dan, A.J. J, R. Kurup, N.S. Pradeep, R.K. Valsamma, V. George, Caryophyllene-rich rhizome oil of Zingiber nimmonii from South India: chemical characterization and antimicrobial activity, Phytochemistry 67 (2006) 2469–2473, https://doi.org/10.1016/j.phytochem.2006.08.003.
[21] A.-L. Klauke, I. Racz, B. Pradier, A. Markert, A.M. Zimmer, J. Gertsch, A. Zimmer, The cannabinoid CB2 receptor-selective phytocannabinoid beta-caryophyllene exerts analgesic effects in mouse models of inflammatory and neuropathic pain, Eur. Neuropsychopharmacol. 24 (2014) 608–620, https://doi.org/10.1016/j.euroneuro.2013.10.008.
[22] J. Legault, A. Pichette, Potentiating effect of β-caryophyllene on anticancer activity of α-humulene, isocaryophyllene and paclitaxel, J. Pharm. Pharmacol. 59 (2010) 1643–1647, https://doi.org/10.1211/jpp.59.12.0005.
[23] M.G. Sarpietro, A. Di Sotto, M.L. Accolla, F. Castelli, Interaction of β-caryophyllene and β-caryophyllene oxide with phospholipid bilayers: differential scanning calorimetry study, Thermochim. Acta 600 (2015) 28–34, https://doi.org/10.1016/j.tca.2014.11.029.
[24] A. Beloqui, M.Á. Solinís, A. Rodríguez-Gascón, A.J. Almeida, V. Préat, Nanostructured lipid carriers: promising drug delivery systems for future clinics, Nanomed. Nanotechnol. Biol. Med. 12 (2016) 143–161, https://doi.org/10.1016/j.nano.2015.09.004.
[25] A. Garcès, M.H. Amaral, J.M. Sousa Lobo, A.C. Silva, Formulations based on solid lipid nanoparticles (SLN) and nanostructured lipid carriers (NLC) for cutaneous use: a review, Eur. J. Pharmaceut. Sci. 112 (2018) 159–167, https://doi.org/10.1016/j.ejps.2017.11.023.
[26] H. Kim, J.T. Kim, S. Barua, S.-Y. Yoo, S.-C. Hong, K. Bin Lee, J. Lee, Seeking better topical delivery technologies of moisturizing agents for enhanced skin

moisturization, Expet Opin. Drug Deliv. 15 (2018) 17–31, https://doi.org/10.1080/17425247.2017.1306054.
[27] M. Sala, R. Diab, A. Elaissari, H. Fessi, Lipid nanocarriers as skin drug delivery systems: properties, mechanisms of skin interactions and medical applications, Int. J. Pharm. 535 (2018) 1–17, https://doi.org/10.1016/j.ijpharm.2017.10.046.
[28] S. Weber, A. Zimmer, J. Pardeike, Solid lipid nanoparticles (SLN) and nanostructured lipid carriers (NLC) for pulmonary application : a review of the state of the art, Eur. J. Pharm. Biopharm. 86 (2014) 7–22, https://doi.org/10.1016/j.ejpb.2013.08.013.
[29] Nações Unidas no Brasil, in: Os Objetivos De Desenvolvimento Sustentável No Brasil: Consumo E Produção Responsáveis, 2025. https://brasil.un.org/pt-br/sdgs/12.
[30] E. Amiel, R. Ofir, N. Dudai, E. Soloway, T. Rabinsky, S. Rachmilevitch, β -Caryophyllene, a compound isolated from the biblical balm of gilead (Commiphora gileadensis), is a selective apoptosis inducer for tumor cell lines, evidence-based complement, Altern. Med. 2012 (2012) 1–8, https://doi.org/10.1155/2012/872394.
[31] J.G. Graham, M.L. Quinn, D.S. Fabricant, N.R. Farnsworth, Plants used against cancer—an extension of the work of Jonathan Hartwell, J. Ethnopharmacol. 73 (2000) 347–377.
[32] J.M. Pezzuto, Plant-derived anticancer agents, Biochem. Pharmacol. 53 (1997) 121–133.
[33] ANVISA, in: 7a EdiçãoFarmacopeia Brasileira, vol. I, Agência Nac. Vigilância Sanitária, 2024, p. 1072. http://bibliotecadigital.anvisa.gov.br/jspui/handle/anvisa/11937.
[34] F. Tamjidi, M. Shahedi, J. Varshosaz, A. Nasirpour, Design and characterization of astaxanthin-loaded nanostructured lipid carriers, Innov. Food Sci. Emerg. Technol. 26 (2014) 366–374, https://doi.org/10.1016/j.ifset.2014.06.012.
[35] F. Fratini, G. Cilia, B. Turchi, A. Felicioli, Beeswax: a minireview of its antimicrobial activity and its application in medicine, Asian Pac. J. Trop. Med. 9 (2016) 839–843, https://doi.org/10.1016/j.apjtm.2016.07.003.
[36] H.R. Hepburn, R.T.F. Bernard, B.C. Davidson, W.J. Muller, P. Lloyd, S.P. Kurstjens, S.L. Vincent, Synthesis and secretion of beeswax in honeybees, Apidologie 22 (1991) 21–36, https://doi.org/10.1051/apido:19910104.
[37] L. Boltri, T. Canal, P.A. Esposito, F. Carli, Lipid nanoparticles: evaluation of some critical formulation parameters, Proc. Int. Symp. Control. Release Bioact. Mater. 20 (1993) 346–347.
[38] M.R. Gasco, Solid lipid nanospheres from warm micro-emulsions, Pharm. Technol. Eur. 9 (1997) 52–58.
[39] R.H. Müller, K. Mäder, S. Gohla, Solid lipid nanoparticles (SLN) for controlled drug delivery - a review of the state of the art, Eur. J. Pharm. Biopharm. 50 (2000) 161–177, https://doi.org/10.1016/S0939-6411(00)00087-4.
[40] Anton Paar GmbH, Manual De Instrução do Instrumento De Espalhamento De Luz Litesizer 500 Para Análise De Partículas, 2016, p. 66.
[41] Merck, User Guide Amicon® Ultra-0.5 Centrifugal Filter Devices for Volumes up to 500 Ml, 2023.
[42] M.C. de Oliveira, M.E.L. Dano, R.S. dos Santos, M. Villa Nova, C.V. Nakamura, W. Caetano, M.L. Bruschi, HPLC analysis of β-caryophyllene in copaiba oleoresin: development, validation and applicability, Res. Soc. Dev. 11 (2022), https://doi.org/10.33448/rsd-v11i10.32525.
[43] M.E.L. Dano, R. Said dos Santos, J. Bassi da Silva, M.V. Junqueira, S.B. de Souza Ferreira, M.L. Bruschi, Design of emulgel platforms for local propolis delivery: the influence of type and concentration of carbomer, J. Mol. Liq. 334 (2021) 116025, https://doi.org/10.1016/j.molliq.2021.116025.
[44] C. Gonçalves, M.J. Ramalho, R. Silva, V. Silva, R. Marques-Oliveira, A.C. Silva, M. C. Pereira, J.A. Loureiro, Lipid nanoparticles containing mixtures of antioxidants to improve skin care and cancer prevention, Pharmaceutics 13 (2021) 2042, https://doi.org/10.3390/pharmaceutics13122042.
[45] C. Jaudoin, M. Maue Gehrke, I. Grillo, F. Cousin, M. Ouldali, A.-A. Arteni, E. Ferrary, F. Siepmann, J. Siepmann, F. Simelière, A. Bochot, F. Agnely, Release of liposomes from hyaluronic acid-based hybrid systems: effects of liposome surface and size, Int. J. Pharm. 648 (2023) 123560, https://doi.org/10.1016/j.ijpharm.2023.123560.
[46] R.R.A. Pereira, Desenvolvimento E Caracterização De Sistema Mucoadesivo Termossensível Contendo Micropartículas De Própolis Para Potential Tratamento De Candidíase Vulvovaginal, Dissertação (Mestrado em ciências farmacêuticas) – Universidade Estadual de Maringá, Maringá, 2011.
[47] M.L. Bruschi, Desenvolvimento E Caracterização De Sistemas De Liberação De Própolis Intrabolsa Periodontal., Tese (Doutorado Em Ciências Farmacêuticas)-Faculdade De Ciências Farmacêuticas De Ribeirão Preto, Universidade de São Paulo, Ribeirão Preto, 2006.
[48] R.W. Korsmeyer, R. Gurny, E. Doelker, P. Buri, N.A. Peppas, Mechanisms of solute release from porous hydrophilic polymers, Int. J. Pharm. 15 (1983) 25–35, https://doi.org/10.1016/0378-5173(83)90064-9.
[49] E. Folzer, D. Gonzalez, R. Singh, H. Derendorf, Comparison of skin permeability for three diclofenac topical formulations: an *in vitro* study, Pharmazie 69 (2014) 27–31. http://www.ncbi.nlm.nih.gov/pubmed/24601219.
[50] R. Said dos Santos, C.F. Vecchi, H.C. Rosseto, J. Bassi da Silva, M.E.L. Dano, L.V. de Castro-Hoshino, M.L. Baesso, M.L. Bruschi, Emulgels containing carbopol 934P and different vegetable oils for topical propolis delivery: bioadhesion, drug release profile, and Ex vivo skin permeation studies, AAPS PharmSciTech 21 (2020) 209, https://doi.org/10.1208/s12249-020-01748-3.
[51] F.Q. Ames, F. Sato, L.V. de Castro, L.L.M. de Arruda, B.A. da Rocha, R.K.N. Cuman, M.L. Baesso, C.A. Bersani-Amado, Evidence of anti-inflammatory effect and percutaneous penetration of a topically applied fish oil preparation: a photoacoustic spectroscopy study, J. Biomed. Opt. 22 (2017) 055003, https://doi.org/10.1117/1.JBO.22.5.055003.
[52] M.L. Baesso, J. Shen, R.D. Snoo, Laser-induced photoacoustic signal phase study of stratum corneum and epidermis, Anal 119 (119) (1994) 561–562.
[53] T. Mosmann, Rapid colorimetric assay for cellular growth and survival: application to proliferation and cytotoxicity assays, J. Immunol. Methods 65 (1983) 55–63, https://doi.org/10.1016/0022-1759(83)90303-4.
[54] D.S. Jones, Pharmaceutical Statistics, The Pharmaceutical Press, Londres, 2002.
[55] Y. Soleimanian, S.A.H. Goli, J. Varshosaz, S.M. Sahafi, Formulation and characterization of novel nanostructured lipid carriers made from beeswax, propolis wax and pomegranate seed oil, Food Chem. 244 (2018) 83–92, https://doi.org/10.1016/j.foodchem.2017.10.010.
[56] U.S. Coast Guard, Chemical Hazard Response Information System (CHRIS) - Hazardous Chemical Data, 1999. Commandant Instruction 16465.12C.
[57] S.R.M. Lima, V.F.V. Junior, H.B. Christo, A.C. Pinto, P.D. Fernandes, *In vivo* and *in vitro* studies on the anticancer activity of Copaifera multijuga hayne and its fractions, Phyther. Res. 17 (2003) 1048–1053, https://doi.org/10.1002/ptr.1295.
[58] J. Pardeike, A. Hommoss, R.H. Müller, Lipid nanoparticles (SLN, NLC) in cosmetic and pharmaceutical dermal products, Int. J. Pharm. 366 (2009) 170–184, https://doi.org/10.1016/j.ijpharm.2008.10.003.
[59] B. Xia, Y. Shen, R. Zhao, J. Deng, C. Wang, Interactions with soy lecithin regulate the emulsification capacity of pea protein: effects of soy lecithin concentration, Food Hydrocoll. 155 (2024) 110168, https://doi.org/10.1016/j.foodhyd.2024.110168.
[60] S. Asadinezhad, F. Khodaiyan, M. Salami, H. Hosseini, B. Ghanbarzadeh, Effect of different parameters on orange oil nanoemulsion particle size: combination of low energy and high energy methods, J. Food Meas. Charact. 13 (2019) 2501–2509, https://doi.org/10.1007/s11694-019-00170-z.
[61] D.J. Mcclements, Critical review of techniques and methodologies for characterization of emulsion stability, Crit. Rev. Food Sci. Nutr. 47 (2007) 611–649, https://doi.org/10.1080/10408390701289292.
[62] A.M. Hashtjin, S. Abbasi, Nano-emulsification of orange peel essential oil using sonication and native gums, Food Hydrocoll. 44 (2015) 40–48, https://doi.org/10.1016/j.foodhyd.2014.08.017.
[63] P.-H. Li, B.-H. Chiang, Process optimization and stability of d-limonene-in-water nanoemulsions prepared by ultrasonic emulsification using response surface methodology, Ultrason. Sonochem. 19 (2012) 192–197, https://doi.org/10.1016/j.ultsonch.2011.05.017.
[64] C.M. Pinto, L.S. Horta, A.P. Soares, B.A. Carvalho, E. Ferreira, E.B. Lages, L.A. M. Ferreira, A.A.G. Faraco, H.C. Santiago, G.A.C. Goulart, Nanoencapsulated Doxorubicin prevents mucositis development in mice, Pharmaceutics 13 (2021) 1021, https://doi.org/10.3390/pharmaceutics13071021.
[65] N. Ayshah Rosli, R. Hasham, A. Abdul Aziz, T. Ubaidah Noh, K. Jemon, Nanostructured lipid carrier loaded with Zingiber officinale oil to enhance transdermal bioactive delivery for topical formulation, Microchem. J. 200 (2024) 110470, https://doi.org/10.1016/j.microc.2024.110470.
[66] N.A. Rosli, G.A. Islan, R. Hasham, G.R. Castro, A. Abdul Aziz, Incorporation of nanoparticles based on Zingiber Officinale essential oil into alginate films for sustained release, J. Phys. Sci. 33 (2022) 107–124, https://doi.org/10.21315/jps2022.33.2.7.
[67] N.A. Peppas, J.J. Sahlin, A simple equation for the description of solute release. III. Coupling of diffusion and relaxation, Int. J. Pharm. 57 (1989) 169–172, https://doi.org/10.1016/0378-5173(89)90306-2.
[68] M.L. Bruschi, Mathematical models of drug release, in: Strateg. to Modify Drug Release from Pharm. Syst., Elsevier, 2015, pp. 63–86, https://doi.org/10.1016/B978-0-08-100092-2.00005-9.
[69] C.M. Lopes, J.M.S. Lobo, P. Costa, Formas farmacêuticas de liberação modificada: polímeros hidrifílicos, Brazilian J. Pharm. Sci. 41 (2005) 143–154.
[70] A.C.V. de Oliveira, F.A.P. de Morais, K. da S.S. Campanholi, D.L. Bidóia, R. B. Balbinot, C.V. Nakamura, W. Caetano, N. Hioka, O. dos S. Monteiro, C.Q. da Rocha, R.S. Gonçalves, Melanoma-targeted photodynamic therapy based on hypericin-loaded multifunctional P123-spermine/folate micelles, Photodiagnosis Photodyn. Ther. 40 (2022) 103103, https://doi.org/10.1016/j.pdpdt.2022.103103.
[71] H.R. Kelidari, H. Alipanah, G. Roozitalab, M. Ebrahimi, M. Osanloo, Anticancer effect of solid-lipid nanoparticles containing Mentha longifolia and Mentha pulegium essential oils: *in Vitro* study on human melanoma and breast cancer cell lines, Biointerface Res. Appl. Chem. 12 (2021) 2128–2137, https://doi.org/10.33263/BRIAC122.21282137.